

NUMERICAL METHODS FOR SPDES WITH TEMPERED STABLE PROCESSES*

MENGDI ZHENG[†] AND GEORGE EM KARNIADAKIS[†]

Abstract. We develop new probabilistic and deterministic approaches for moment statistics of stochastic partial differential equations with pure jump tempered α -stable (T α S) Lévy processes. With the compound Poisson (CP) approximation or the series representation of the T α S process, we simulate the moment statistics of stochastic reaction-diffusion equations with additive T α S white noises by the probability collocation method (PCM) and the Monte Carlo (MC) method. PCM is shown to be more efficient and accurate than MC in relatively low dimensions. Then as an alternative approach, we solve the generalized Fokker–Planck equation that describes the evolution of the density for stochastic overdamped Langevin equations to obtain the density and the moment statistics for the solution following two different approaches. First, we solve an integral equation for the density by approximating the T α S processes as CP processes; second, we directly solve the tempered fractional PDE (TFPDE). We show that the numerical solution of TFPDE achieves higher accuracy than PCM at a lower cost and we also demonstrate agreement between the histogram from MC and the density from the TFPDE.

Key words. generalized polynomial chaos, white noise, Fokker–Planck equation, tempered fractional PDE

AMS subject classifications. 35R11, 60G51, 60H15, 60H40

DOI. 10.1137/140966083

1. Introduction. We develop and compare different numerical methods to solve two stochastic models with tempered α -stable (T α S) Lévy white noises: a reaction-diffusion equation and an overdamped Langevin equation with T α S white noises, including stochastic simulation methods such as the Monte Carlo (MC) [11, 43] and probability collocation method (PCM) [3, 55]. We also simulate the density of the overdamped Langevin equation through its generalized Fokker–Planck (FP) equation formulated as a tempered fractional PDE (TFPDE).

1.1. Stochastic models driven by tempered stable white noises. We first solve the following stochastic reaction-diffusion model via stochastic simulation methods (MC and PCM) in the Itô sense:

$$(1.1) \quad \begin{cases} du(t, x; \omega) = \left(\frac{\partial^2 u}{\partial x^2} + \mu u \right) dt + \epsilon dL_t(\omega), & x \in [0, 2], \\ u(t, 0) = u(t, 2), & \text{periodic boundary condition,} \\ u(0, x) = u_0(x) = \sin\left(\frac{\pi}{2}x\right), & \text{initial condition,} \end{cases}$$

where $L_t(\omega)$ is a one-dimensional T α S process (also known as a Carr–Geman–Madan–Yor (CGMY) process in finance) [9, 10].

The second model is a one-dimensional stochastic overdamped Langevin equation in the Itô sense [12, 24]:

$$(1.2) \quad dx(t; \omega) = -\sigma x(t; \omega) dt + dL_t(\omega), \quad x(0) = x_0,$$

*Submitted to the journal’s Methods and Algorithms for Scientific Computing section April 21, 2014; accepted for publication (in revised form) February 12, 2015; published electronically May 5, 2015. This work was partially supported by OSD-MURI (grant FA9550-09-1-0613), NSF/DMS (grant DMS-1216437), and the new DOE Center on Mathematics for Mesoscopic Modeling of Materials (CM4).

<http://www.siam.org/journals/sisc/37-3/96608.html>

[†]Division of Applied Mathematics, Brown University, Providence, RI 02906 (mengdi_zheng@brown.edu, george_karniadakis@brown.edu).

where $L_t(\omega)$ is also a one-dimensional T α S process. It describes an overdamped particle in an external potential driven by additive T α S white noise. This equation was introduced in [28] to describe the stochastic dynamics in fluctuating environments for Gaussian white noise, such as classical mechanics [20], biology [22], and finance [11]. When $L_t(\omega)$ is a Lévy process, the solution is a Markov process and its probability density satisfies a closed equation such as the differential Chapman–Kolmogorov equation [15] or the generalized FP equation [47]. When $L_t(\omega)$ is a T α S Lévy process, the corresponding generalized FP equation is a TFPDE [12].

1.2. Background on tempered stable processes. T α S processes were introduced in statistical physics to model turbulence, e.g., the truncated Lévy flight model [27, 33, 39], and in mathematical finance to model stochastic volatility, e.g., the CGMY model [9, 10]. Here, we consider a symmetric T α S process (L_t) as a pure jump Lévy martingale with characteristic triplet $(0, \nu, 0)$ [6, 52] (no drift and no Gaussian part). The Lévy measure is given¹ by [11]

$$(1.3) \quad \nu(x) = \frac{ce^{-\lambda|x|}}{|x|^{\alpha+1}}, \quad 0 < \alpha < 2.$$

This Lévy measure can be interpreted as an Esscher transformation [18] from that of a stable process with exponential tilting of the Lévy measure. The parameter $c > 0$ alters the intensity of jumps of all given sizes; it changes the time scale of the process. Also, $\lambda > 0$ fixes the decay rate of big jumps, while α determines the relative importance of smaller jumps in the path of the process.² The probability density for L_t at a given time is not available in a closed form (except when $\alpha = \frac{1}{2}$).³ The characteristic exponent for L_t is [11]

$$(1.4) \quad \Phi(s) = s^{-1} \log \mathbf{E}[e^{isL_s}] = 2\Gamma(-\alpha)\lambda^\alpha c \left[\left(1 - \frac{is}{\lambda}\right)^\alpha - 1 + \frac{is\alpha}{\lambda} \right], \quad \alpha \neq 1,$$

where $\Gamma(x)$ is the Gamma function and \mathbf{E} is the expectation. By taking the derivatives of the characteristic exponent we obtain the mean and variance:

$$(1.5) \quad \mathbf{E}[L_t] = 0, \quad \text{Var}[L_t] = 2t\Gamma(2 - \alpha)c\lambda^{\alpha-2}.$$

In order to derive the second moments for the exact solutions of (1.1) and (1.2), we introduce the Itô isometry. The *jump* of L_t is defined by $\Delta L_t = L_t - L_{t-}$. We define the *Poisson random measure* $N(t, U)$ as [23, 37, 40]

$$(1.6) \quad N(t, U) = \sum_{0 \leq s \leq t} \mathbf{I}_{\Delta L_s \in U}, \quad U \in \mathcal{B}(\mathbf{R}_0), \quad \bar{U} \subset \mathbf{R}_0.$$

Here $\mathbf{R}_0 = \mathbf{R} \setminus \{0\}$, and $\mathcal{B}(\mathbf{R}_0)$ is the σ -algebra generated by the family of all Borel subsets $U \subset \mathbf{R}$, such that $\bar{U} \subset \mathbf{R}_0$; \mathbf{I}_A is an indicator function. The Poisson random measure $N(t, U)$ counts the number of jumps of size $\Delta L_s \in U$ at time t . In order to introduce the Itô isometry, we define the *compensated Poisson random measure* \tilde{N} [23] as

$$(1.7) \quad \tilde{N}(dt, dz) = N(dt, dz) - \nu(dz)dt = N(dt, dz) - \mathbf{E}[N(dt, dz)].$$

¹In a more generalized form, the Lévy measure is $\nu(x) = \frac{c_- e^{-\lambda_- |x|}}{|x|^{\alpha+1}} \mathbf{I}_{x < 0} + \frac{c_+ e^{-\lambda_+ |x|}}{|x|^{\alpha+1}} \mathbf{I}_{x > 0}$. We may have different coefficients $c_+, c_-, \lambda_+, \lambda_-$ on the positive and the negative jump parts.

²In the case when $\alpha = 0$, L_t is the gamma process.

³See inverse Gaussian processes.

The TαS process L_t (as a martingale) can be also written as

$$(1.8) \quad L_t = \int_0^t \int_{\mathbf{R}_0} z \tilde{N}(d\tau, dz).$$

For any t , let \mathcal{F}_t be the σ -algebra generated by $(L_s, \tilde{N}(ds, dz))$, $z \in \mathbf{R}_0$, $s \leq t$. We define the filtration to be $\mathbf{F} = \{\mathcal{F}_t, t \geq 0\}$. If a stochastic process $\theta_t(z), t \geq 0, z \in \mathbf{R}_0$ is \mathcal{F}_t -adapted, we have the following Itô isometry [37]:

$$(1.9) \quad \mathbf{E} \left[\left(\int_0^T \int_{\mathbf{R}_0} \theta_t(z) \tilde{N}(dt, dz) \right)^2 \right] = \mathbf{E} \left[\int_0^T \int_{\mathbf{R}_0} \theta_t^2(z) \nu(dz) dt \right].$$

Equations (1.1) and (1.2) are understood in the Itô sense. The solutions are stochastic Itô integrals over the TαS processes L_t [46], such as $\int_0^T f(t) dL_t$, with the Lévy measure given in (1.3). Thus, by applying (1.8), the second moment can be derived using the Lévy measure:

$$(1.10) \quad \begin{aligned} \mathbf{E} \left[\left(\int_0^T f(t) dL_t \right)^2 \right] &= \mathbf{E} \left[\left(\int_0^T \int_{\mathbf{R}_0} f(t) z \tilde{N}(dt, dz) \right)^2 \right] \\ &= \mathbf{E} \left[\int_0^T \int_{\mathbf{R}_0} f^2(t) z^2 \nu(dz) dt \right]. \end{aligned}$$

Both equations (1.1) and (1.2) contain an additive white noise \dot{L}_t of a TαS process. Details of white noise theory for Lévy processes with applications to stochastic partial differential equations (SPDEs) and finance can be found in [5, 38, 30, 31, 41]. The white noise of a Poisson random measure takes values in a certain distribution space. It is constructed via a chaos expansion for Lévy processes with kernels of polynomial type [38], and defined as a chaos expansion in terms of iterated integrals with respect to the compensated Poisson measure $\tilde{N}(dt, dz)$ [25].

1.3. Numerical simulations of functionals of TαS processes. For simulations of TαS Lévy processes, we do not know the distribution of increments explicitly [11], but we may still simulate the trajectories of TαS processes by the random walk approximation [4]. However, the random walk approximation does not identify the jump time and size of the large jumps precisely [48, 49, 50, 51]. In the heavy tailed case, large jumps contribute more than small jumps in functionals of a Lévy process. Therefore, in this case, we have mainly used two other ways to simulate the trajectories of a TαS process numerically: compound Poisson (CP) approximation [11] and series representation [49]. In the CP approximation, we treat the jumps smaller than a certain size δ by their expectation, and treat the remaining process with larger jumps as a CP process [11]. There are six different series representations of Lévy jump processes. They are the inverse Lévy measure method [14, 26], LePage’s method [29], Bondesson’s method [8], thinning method [49], rejection method [48], and shot noise method [49, 50]. In this paper, for TαS processes, we will use the shot noise representation for L_t as a series representation method because the tail of the Lévy measure of a TαS process does not have an explicit inverse [51]. Both the CP and the series approximation converge slowly when the jumps of the Lévy process are highly concentrated around zero, however, both can be improved by replacing the

small jumps with Brownian motions [2]. The α -stable distribution was introduced to model the empirical distribution of asset prices [32], replacing the normal distribution. The empirical distribution of asset prices is not always in a stable distribution or a normal distribution. The tail is heavier than a normal distribution and thinner than a stable distribution [7]. Therefore, the T α S process was introduced as the CGMY model to modify the Black and Scholes model.

In the past literature, the simulation of SDEs or functionals of T α S processes was mainly done via MC [43]. MC simulation for functionals of T α S processes is possible after a change of measure that transforms T α S processes into stable processes [45].

The paper is organized as follows: in section 2, we compare the CP approximation and the series representation of a T α S process; in section 3, we solve a stochastic reaction-diffusion model with T α S white noise via MC and PCM, both with CP approximation or series representation, of the T α S process; in section 4, we simulate the density evolution for an overdamped Langevin equation with T α S white noise via the corresponding generalized FP equations. We also compare the statistics obtained from the FP equations and MC or PCM methods. We conclude in section 5. In Appendices A and B, we provide algorithms of the rejection method and simulation of CP processes. We also provide the probability distributions to simplify the series representation in Appendix C.

2. Numerical simulation of T α S processes. In general there are three ways to generate a Lévy process [49]: random walk approximation, series representation, and CP approximation. For a T α S process, the distribution of increments is not explicitly known (except for $\alpha = 1/2$) [11]. Therefore, in the following we discuss the CP approximation and the series representation for a T α S process.

2.1. Simulation of T α S processes by CP approximation. In the CP approximation, we simulate the jumps larger than δ as a CP process and replace jumps smaller than δ by their expectation as a drift term [11]. Here we explain the method to approximate a T α S subordinator X_t (without a Gaussian part and a drift) with the Lévy measure $\nu(x) = \frac{ce^{-\lambda x}}{x^{\alpha+1}}\mathbf{I}_{x>0}$ (positive jumps only); this method can be generalized to a T α S process with both positive and negative jumps. The CP approximation X_t^δ for this T α S subordinator X_t is

$$(2.1) \quad \begin{aligned} X_t &\approx X_t^\delta = \sum_{s \leq t} \Delta X_s I_{\Delta X_s \geq \delta} + \mathbf{E} \left[\sum_{s \leq t} \Delta X_s I_{\Delta X_s < \delta} \right] \\ &= \sum_{i=1}^{\infty} J_i^\delta \mathbf{I}_{t \leq T_i} + b^\delta t \approx \sum_{i=1}^{Q_{cp}} J_i^\delta \mathbf{I}_{t \leq T_i} + b^\delta t. \end{aligned}$$

We introduce Q_{cp} here as the number of jumps that occurred before time t . The first term $\sum_{i=1}^{\infty} J_i^\delta \mathbf{I}_{t \leq T_i}$ is a compound Poisson process with jump intensity

$$(2.2) \quad U(\delta) = c \int_{\delta}^{\infty} \frac{e^{-\lambda x} dx}{x^{\alpha+1}}$$

and jump size distribution $p^\delta(x) = \frac{1}{U(\delta)} \frac{ce^{-\lambda x}}{x^{\alpha+1}} \mathbf{I}_{x \geq \delta}$ for J_i^δ . The jump size random variables (RVs) J_i^δ are generated via the rejection method [13], given in Appendix A. Here, T_i is the i th jump arrival time of a Poisson process with intensity $U(\delta)$. The accuracy of the CP approximation method can be improved by replacing the smaller jumps

by a Brownian motion [2], when the growth of the Lévy measure near zero is fast. The second term functions as a drift term, $b^\delta t$, resulting from truncating the smaller jumps. The drift is $b^\delta = c \int_0^\delta \frac{e^{-\lambda x} dx}{x^\alpha}$. This integration diverges when $\alpha \geq 1$, therefore the CP approximation method only applies to T α S processes with $0 < \alpha < 1$. In this paper, both the intensity $U(\delta)$ and drift b^δ are calculated via numerical integrations with Gauss-quadrature rules [16] with a specified relative tolerance (RelTol).⁴ In general, there are two algorithms to simulate a compound Poisson process [11]: the first method is to simulate the jump time T_i by exponentially distributed RVs and take the number of jumps Q_{cp} as large as possible; the second method is to first generate and fix the number of jumps, then generate the jump time by uniformly distributed RVs on $[0, t]$. Algorithms for simulating a CP process (the second kind) with intensity and the jump size distribution in their explicit forms are known on a fixed time grid [11], given in Appendix B. In order to simulate the sample paths of a symmetric T α S process with a Lévy measure given in (1.3), we generate two independent T α S subordinators via the CP approximation and subtract one from the other. The accuracy of the CP approximation is determined by the jump truncation size δ .

2.2. Simulation of T α S processes by series representation. Let $\{\epsilon_j\}$, $\{\eta_j\}$, and $\{\xi_j\}$ be sequences of independently and identically distributed (i.i.d.) RVs such that $\mathbf{P}(\epsilon_j = \pm 1) = 1/2$, $\eta_j \sim \text{Exponential}(\lambda)$, and $\xi_j \sim \text{Uniform}(0, 1)$. Let $\{\Gamma_j\}$ be arrival times in a Poisson process with rate one. Let $\{U_j\}$ be i.i.d. uniform RVs on $[0, T]$. Then, a T α S process L_t with Lévy measure given in (1.3) can be represented as [51]

$$(2.3) \quad L_t = \sum_{j=1}^{+\infty} \epsilon_j \left[\left(\frac{\alpha \Gamma_j}{2cT} \right)^{-1/\alpha} \wedge \eta_j \xi_j^{1/\alpha} \right] \mathbf{I}_{\{U_j \leq t\}}, \quad 0 \leq t \leq T.$$

Equation (2.3) converges almost surely as uniformly in t [48]. In numerical simulations, we truncate the series in (2.3) up to Q_s terms. The accuracy of a series representation approximation is determined by the number of truncations Q_s .

2.3. Simulating inverse Gaussian (IG) subordinators ($\alpha = 1/2$). In order to compare the numerical performance of CP approximation and series representation of T α S processes, we simulate the trajectories of an IG subordinator by the two methods. An IG subordinator is a T α S subordinator with a Lévy measure (with one-sided jumps, $\alpha = 1/2$) as

$$(2.4) \quad \nu_{IG} = \frac{ce^{-\lambda x}}{x^{3/2}} \mathbf{I}_{x>0}.$$

The probability density function (PDF) at time t for an IG subordinator is known to be [11]

$$(2.5) \quad p_t(x) = \frac{ct}{x^{3/2}} e^{2ct\sqrt{\pi\lambda}} e^{-\lambda x - \pi c^2 t^2/x}, \quad x > 0.$$

We perform the *one-sample Kolmogorov–Smirnov statistic (K-S test)* [34] between the empirical cumulative distribution function (CDF) and the exact reference CDF:

$$(2.6) \quad KS = \sup_x |F_{em}(x) - F_{ex}(x)|, \quad x \in \text{supp}(F).$$

⁴The RelTol of numerical integration is defined as $\frac{|q-Q|}{|Q|}$, where q is the computed value of the integral and Q is the unknown exact value.

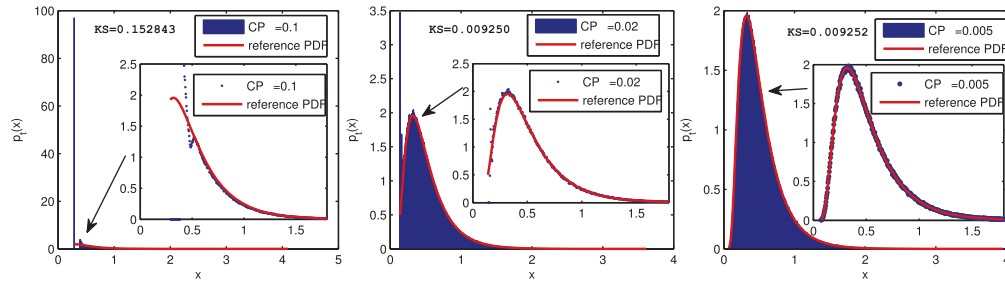


FIG. 1. Empirical histograms of an IG subordinator ($\alpha = 1/2$) simulated via the CP approximation at $t = 0.5$: the IG subordinator has $c = 1$, $\lambda = 3$; each simulation contains $s = 10^6$ samples (we zoom in and plot $x \in [0, 1.8]$ to examine the smaller jumps approximation); they have different jump truncation sizes as $\delta = 0.1$ (left, dotted, CPU time 1450 s), $\delta = 0.02$ (middle, dotted, CPU time 5710 s), and $\delta = 0.005$ (right, dotted, CPU time 38531 s). The reference PDFs are plotted in red solid lines; the one-sample K-S test values are calculated for each plot; the RelTol of integration in $U(\delta)$ and b^δ is 1×10^{-8} . These runs were done on Intel (R) Core (TM) i5-3470 CPU @ 3.20 GHz in MATLAB.

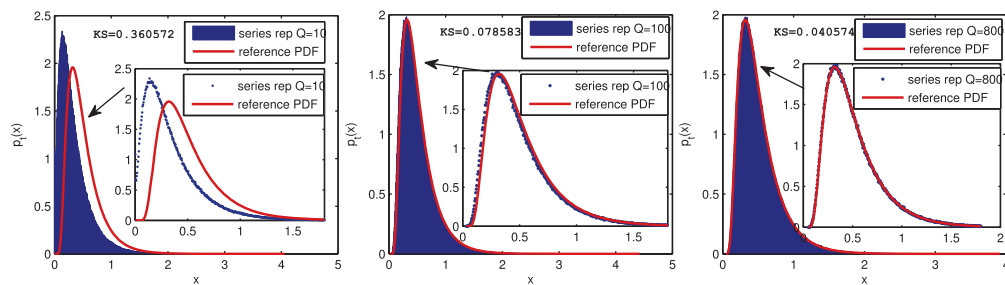


FIG. 2. Empirical histograms of an IG subordinator ($\alpha = 1/2$) simulated via the series representation at $t = 0.5$: the IG subordinator has $c = 1$, $\lambda = 3$; each simulation is done on the time domain $[0, 0.5]$ and contains $s = 10^6$ samples (we zoom in and plot $x \in [0, 1.8]$ to examine the smaller jumps approximation); they have different numbers of truncations in the series as $Q_s = 10$ (left, dotted, CPU time 129 s), $Q_s = 100$ (middle, dotted, CPU time 338 s), and $Q_s = 1000$ (right, dotted, CPU time 2574 s). The reference PDFs are plotted in red solid lines; the one-sample K-S test values are calculated for each plot. These runs were done on Intel (R) Core (TM) i5-3470 CPU @ 3.20 GHz in MATLAB.

This one-sample K-S test quantifies a distance between the exact IG process and the approximated one (by the CP approximation or the series representation).

In Figures 1 and 2, we plot the empirical histograms (with the area normalized to one) of an IG subordinator at time t , simulated via the CP approximation with different small jump truncation sizes δ (explained in section 2.1) and via the series representation with different numbers of truncations in the series Q_s (explained in section 2.2), against the reference PDF in (2.5). We observe that the empirical histograms fit the reference PDF better when $\delta \rightarrow 0$ in the CP approximation in Figure 1 and when Q_s increases in the series representation. The quality of fitting is shown quantitatively via the K-S test values given in each plot.

In both Figures 1 and 2, we run one million samples on 1000 bins for each histogram (known as the square-root choice [54]). We zoom in and plot the parts of histograms on $[0, 1.8]$ to examine how smaller jumps are captured. We observe that in both Figures 1 and 2 when δ is large or Q_s is small, the distribution of small jumps is not well approximated. Therefore, both methods suffer from accuracy if smaller

jumps have a big contribution to the solution of SPDEs, e.g., when α or λ is large. Furthermore, when δ is large in the CP approximation (see $\delta = 0.1$ in Figure 1), the big jumps are well approximated although the small ones are not; when Q_s is small in the series representation, neither big nor small jumps are well approximated (see $Q_s = 10$ in Figure 2). When the cost is limited, this shows an advantage of using the CP approximation, when big jumps have a larger contribution to the solution of SPDEs.

3. Simulation of reaction-diffusion equations with T α S white noises.

In this section, we will provide numerical results for solving the stochastic reaction-diffusion equation (1.1). We will perform and compare four stochastic simulation methods to obtain the statistics: MC with CP approximation (MC/CP), MC with series representation (MC/S), PCM with CP approximation (MC/CP), and PCM with series representation (PCM/S).

The integral form of (1.1) is

$$(3.1) \quad u(t, x) = e^{\mu t - \frac{\alpha^2}{4}t} \sin\left(\frac{\pi}{2}x\right) + \epsilon e^{\mu t} \int_0^t e^{-\mu\tau} dL_\tau, \quad x \in [0, 2],$$

where the stochastic integral is an Itô integral over a T α S process [46]. The mean of the solution is

$$(3.2) \quad \mathbf{E}_{ex}[u(t, x)] = e^{\mu t - \frac{\alpha^2}{4}t} \sin\left(\frac{\pi}{2}x\right).$$

By the Itô isometry [37] and (3.2), the second moment of the solution is

$$(3.3) \quad \mathbf{E}_{ex}[u^2(t, x; \omega)] = e^{2\mu t - \frac{\alpha^2}{2}t} \sin^2\left(\frac{\pi}{2}x\right) + \frac{c\epsilon^2 e^{2\mu t}}{\mu\lambda^{2-\alpha}} (1 - e^{-2\mu t})\Gamma(2 - \alpha).$$

Let us define the L_2 norm of the error in the second moment $l2u2(t)$ to be

$$(3.4) \quad l2u2(t) = \frac{\|\mathbf{E}_{ex}[u^2(x, t; \omega)] - \mathbf{E}_{num}[u^2(x, t; \omega)]\|_{L_2([0,2])}}{\|\mathbf{E}_{ex}[u^2(x, t; \omega)]\|_{L_2([0,2])}},$$

where $E_{num}[u^2(x, t; \omega)]$ is the second moment evaluated by numerical simulations.

3.1. Comparing CP approximation and series representation in MC.

First we will compare the accuracy and convergence rate between MC/CP and MC/S in solving (1.1) by MC. In MC, we generate the trajectories of L_t (a T α S process with the Levy measure given in (1.3)) on a fixed time grid with st the number of time steps ($\{t_0 = 0, t_1, t_2, \dots, t_{st} = T\}$). We solve (1.1) via the first-order Euler’s method [43] in the time direction with a time step $\Delta t = t^{n+1} - t^n$:

$$(3.5) \quad u^{n+1} - u^n = \left(\frac{\partial^2 u^n}{\partial x^2} + \mu u^n\right) \Delta t + \epsilon(L_{t^{n+1}} - L_{t^n}).$$

We discretize the space by $N_x = 500$ Fourier collocation points [21] on the domain $[0, 2]$.

In Table 1, we plot the $l2u2$ errors at a fixed time T versus the sample size s by the MC/CP and the MC/S, for $\lambda = 10$ (upper) and for $\lambda = 1$ (lower, with a less tempered tail). First for the cost, the MC/CP costs less CPU time than the MC/S, e.g., when $\lambda = 10$ in Table 1, the MC/S with $Q_s = 10$ and $s = 65536$ takes twice the

TABLE 1

MC/CP vs. MC/S: error $l2u2(T)$ of the solution for (1.1) versus the number of samples s with $\lambda = 10$ (upper) and $\lambda = 1$ (lower). $T = 1$, $c = 0.1$, $\alpha = 0.5$, $\epsilon = 0.1$, $\mu = 2$ (upper and lower). Spatial discretization: $N_x = 500$ Fourier collocation points on $[0, 2]$; temporal discretization: first-order Euler scheme in (3.5) with time steps $\Delta t = 1 \times 10^{-5}$. In the CP approximation, $RelTol = 1 \times 10^{-8}$ for integration in $U(\delta)$.

s ($\lambda = 10$)	256	1024	4096	16384	65536	262144
MC/S $Q_s = 10$	3.9×10^{-3}	6.0×10^{-4}	1.6×10^{-4}	6.8×10^{-5}	2.3×10^{-5}	3.5×10^{-6}
MC/CP $\delta = 0.1$	5.4×10^{-4}	6.2×10^{-4}	6.3×10^{-4}	4.3×10^{-4}	4.3×10^{-4}	4.5×10^{-4}
MC/CP $\delta = 0.01$	3.6×10^{-4}	1.8×10^{-5}	9.8×10^{-5}	1.3×10^{-5}	3.5×10^{-6}	2.0×10^{-5}
s ($\lambda = 1$)	256	1024	4096	16384	65536	262144
MC/S $Q_s = 10$	1.7×10^{-2}	1.4×10^{-2}	6.1×10^{-3}	7.6×10^{-3}	4.4×10^{-3}	6.6×10^{-4}
MC/CP $\delta = 0.1$	1.8×10^{-3}	4.9×10^{-3}	2.4×10^{-3}	2.5×10^{-3}	5.1×10^{-4}	2.7×10^{-4}
MC/CP $\delta = 0.01$	8.6×10^{-3}	3.8×10^{-3}	5.8×10^{-3}	2.0×10^{-3}	1.1×10^{-4}	3.6×10^{-5}

CPU time as the MC/CP with $\delta = 0.01$ and $s = 65536$ even though the MC/CP is more accurate. Second, to assess the accuracy of the methods, the MC/CP is more accurate than MC/S even though it takes about half the CPU time, e.g., the MC/CP with $\delta = 0.01$ and the MC/S with $Q_s = 10$. Third, we observe that decreasing δ in the MC/CP to improve the accuracy is more effective with a small s when more smaller jumps are present (larger λ). For example, when $\lambda = 10$, $\delta = 0.01$ starts to be more accurate than $\delta = 0.1$ when $s = 1024$; when $\lambda = 10$, $\delta = 0.01$ starts to be more accurate than $\delta = 0.1$ when $s = 65536$. This can be explained by the fact that large jumps have a greater contribution to the solution and decreasing δ in the MC/CP makes a great difference in sampling smaller jumps as in Figure 1.

3.2. Comparing CP approximation and series representation in PCM.

Next, we will compare the accuracy and efficiency of PCM/CP and PCM/S in solving (1.1). In order to evaluate the moments of solutions, PCM [55], as an integration method on the random space, is based on the Gauss-quadrature rules [16]. Suppose the solution is a function of a finite number of independent RVs ($\{Y^1, Y^2, \dots, Y^n\}$) as $v(Y^1, Y^2, \dots, Y^n)$, the m th moment of the solution, is evaluated by

$$(3.6) \quad \mathbf{E}[v^m(Y^1, Y^2, \dots, Y^n)] = \sum_{i_1=1}^{d_1} \dots \sum_{i_n=1}^{d_n} v^m(y_{i_1}^1, y_{i_2}^2, \dots, y_{i_n}^n) w_{i_1}^1 \dots w_{i_n}^n,$$

where $w_{i_j}^j$ and $y_{i_j}^j$ are the i_j th Gauss-quadrature weight and collocation point for Y^j , respectively. The simulations are run on $(\prod_{i=1}^n d_i)$ deterministic sample points $(y_{i_1}^1, \dots, y_{i_n}^n)$ in the n -dimensional random space. In the CP approximation, the T α S process L_t is approximated via $L_t \approx \sum_{i=1}^{Q_{cp}} J_i^\delta \mathbf{I}_{t \leq T_i} + b^\delta t$, where Q_{cp} is the number of jumps we consider. As we mentioned in section 2.1 there are two ways to simulate a compound Poisson process. Here we treat the number of jumps Q_{cp} as a modeling parameter by the CP approximation and simulate the time between two jumps $T_{i+1} - T_i$ by exponentially distributed RVs with intensity $U(\delta)$. The PCM/CP method contains two parameters: the jump truncation size δ and the number of jumps we consider Q_{cp} . Therefore, the PCM/CP simulations of problem (1.1) are run on the collocation points for RVs J_i^δ and T_i in the $2Q_{cp}$ -dimensional random space (with $d^{2Q_{cp}}$ sample points); Q_{cp} is the number of jumps truncated. In the series representation, the T α S process L_t is approximated via $L_t \approx \sum_{j=1}^{Q_s} \epsilon_j [(\frac{\alpha \Gamma_j}{2cT})^{-1/\alpha} \wedge \eta_j \xi_j^{1/\alpha}] \mathbf{I}_{\{U_j \leq t\}}$ on the simulation

domain $[0, T]$. To reduce the number of RVs (therefore, to decrease the number of dimensions in the random space), we calculate the distribution of $[(\frac{\alpha\Gamma_j}{2cT})^{-1/\alpha} \wedge \eta_j \xi_j^{1/\alpha}]$ for a fixed j in Appendix C and treat it as one RV for each j . Therefore, the PCM/S simulations under the series representation are run on the quadrature points for RVs ϵ_j , $[(\frac{\alpha\Gamma_j}{2cT})^{-1/\alpha} \wedge \eta_j \xi_j^{1/\alpha}]$, and U_j in the $3Q_s$ -dimensional random space (with d^{3Q_s} sample points). In the following, we generate the stochastic collocation points numerically based on the moments [42]. In Appendix D we introduce a method to generate orthogonal polynomials for a given measure with finite moments [56]. The stochastic collocation points are generated by the Gaussian quadrature rule [19]. Alternative methods can also be used such as the Stieltjes' method and the modified Chebyshev method [17]. Here, we assume each RV has the same number of collocation points d .

However, typically for this problem (1.1) we only need $d(Q_{cp} + 1)$ sample points in PCM/CP instead of $d^{2Q_{cp}}$ and only dQ_s sample points in PCM/S instead of d^{3Q_s} . Using the CP approximation given in (2.1), the second moment of the solution in (3.1) can be approximated by

$$(3.7) \quad \mathbf{E}[u^2(t, x; \omega)] \approx e^{2\mu t - \frac{1}{2}\pi^2 t} \sin^2\left(\frac{\pi}{2}x\right) + \epsilon^2 e^{2\mu t} \mathbf{E}[(J_1^\delta)^2] \sum_{i=1}^{Q_{cp}} \mathbf{E}[e^{-2\mu T_i}].$$

Using the series representation given in (2.3), the second moment of the solution in (3.1) can be approximated by

$$(3.8) \quad \mathbf{E}[u^2(t, x; \omega)] \approx e^{2\mu t - \frac{1}{2}\pi^2 t} \sin^2\left(\frac{\pi}{2}x\right) + \epsilon^2 e^{2\mu t} \frac{1}{2\mu T} (1 - e^{-2\mu T}) \sum_{j=1}^{Q_s} \mathbf{E} \left[\left(\left(\frac{\alpha\Gamma_j}{2cT} \right)^{-1/\alpha} \wedge \eta_j \xi_j^{1/\alpha} \right)^2 \right].$$

The distribution of RV $[(\frac{\alpha\Gamma_j}{2cT})^{-1/\alpha} \wedge \eta_j \xi_j^{1/\alpha}]$ is given in Appendix C. Here we sample the moments of solution directly from (3.7) for the PCM/CP and (3.8) for the PCM/S; therefore, we significantly decrease the sample size with the integral form of the solution in (3.1). For example, in this typical problem we may evaluate $\mathbf{E}[e^{-2\mu T_i}]$ for each i separately in (3.7). Indeed, such a reduction of the number of samples in the PCM method is possible whenever the following condition can be met. Suppose we have Q independent RVs $\{Z_i, i = 1, \dots, Q\}$. If the expectation of a functional of $\{Z_i, i = 1, \dots, Q\}$ is a functional of expectation of some function of each Z_i separately,

$$(3.9) \quad E[F(Z_1, \dots, Z_d)] = G(E[f_1(Z_1)], \dots, E[f_d(Z_d)]),$$

we may evaluate each $E[f_i(Z_i)]$ “separately” via the PCM with d collocation points. In this way, we reduce the number of samples from d^Q to dQ .

In Figure 3, we plot the $l2u2(T)$ errors of the solution for (1.1) versus the number of jumps Q_{cp} (via PCM/CP) or Q_s (via PCM/S). In order to investigate the Q_{cp} and Q_s convergence, we apply a sufficient number of collocation points for each RV until the integration is up to a certain *RelTol*. We observe three things in Figure 3.

1. For smaller values of Q_s and Q_{cp} , PCM/S is more accurate and converges faster than PCM/CP, because bigger jumps contribute more to the solution and PCM/S samples bigger jumps more efficiently than PCM/CP as we observed in Figures 1 and 2.

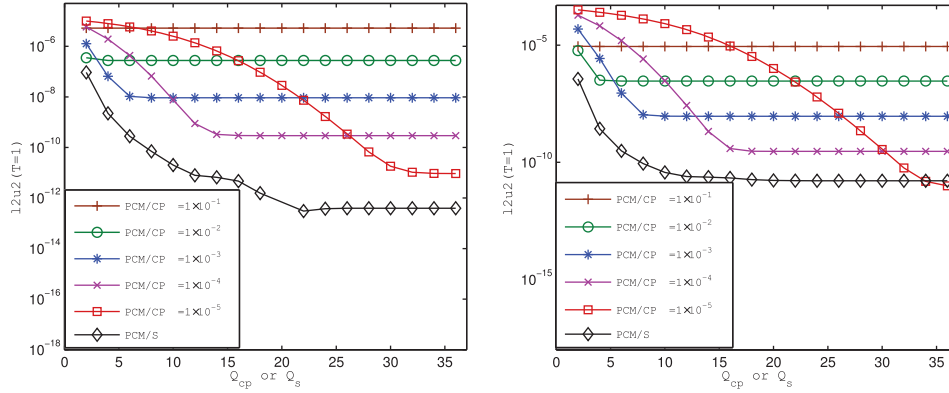


FIG. 3. PCM/CP vs. PCM/S: error $l2u2(T)$ of the solution for (1.1) versus the number of jumps Q_{cp} (in PCM/CP) or Q_s (in PCM/S) with $\lambda = 10$ (left) and $\lambda = 1$ (right). $T = 1$, $c = 0.1$, $\alpha = 0.5$, $\epsilon = 0.1$, $\mu = 2$, $N_x = 500$ Fourier collocation points on $[0, 2]$ (left and right). In the PCM/CP, $RelTol = 1 \times 10^{-10}$ for integration in $U(\delta)$. In the PCM/S, $RelTol = 1 \times 10^{-8}$ for the integration of $\mathbf{E}[(\frac{\alpha \Gamma_j}{2cT})^{-1/\alpha} \wedge \eta_j \xi_j^{1/\alpha}]^2$.

2. For intermediate values of Q_s and Q_{cp} , the convergence rate of PCM/S slows down but the convergence rate of PCM/CP speeds up, because the contribution of smaller jumps starts to affect the accuracy since the PCM/CP samples the smaller jumps faster than PCM/S.
3. For larger values of Q_s and Q_{cp} , both PCM/CP and PCM/S stop converging due to their own limitations to achieve higher accuracy.

The limitations of PCM/CP and PCM/S are

- in the PCM/CP when δ is small, the integration to calculate $U(\delta) = c \int_{\delta}^{\infty} \frac{e^{-\lambda x}}{x^{\alpha+1}} dx$ is less accurate because of the singularity of the integrand at 0;
- in the PCM/S, the density for the RV $[(\frac{\alpha \Gamma_j}{2cT})^{-1/\alpha} \wedge \eta_j \xi_j^{1/\alpha}]$ in (2.3) for a greater value of j requires more collocation points (d) to accurately approximate the expectation of any functionals of $[(\frac{\alpha \Gamma_j}{2cT})^{-1/\alpha} \wedge \eta_j \xi_j^{1/\alpha}]$.

Within their own limitations (δ not too small, Q_s not too large), the PCM/S achieves higher accuracy than the PCM/CP; however, it costs much more computational time especially when the T α S process L_t contains more smaller jumps. For example, when $\lambda = 10$ in Figure 3, to achieve the same accuracy of 10^{-11} , the PCM/S with $Q_s = 10$ costs more than 100 times the CPU time than the PCM/CP with $Q_{cp} = 30$ and $\delta = 1 \times 10^{-5}$.

3.3. Comparing MC and PCM in CP approximation or series representation. Next we compare the accuracy and efficiency both between MC/CP and PCM/CP and between MC/S and PCM/S to obtain the statistics of the solution of (1.1).

In Figure 4, we compare MC/CP and PCM/CP with the same δ (left), then we compare MC/S and PCM/S (right). In the PCM/CP, we fix d (the number of collocation points for each RV) and vary Q_{cp} to obtain different numbers of sample points s ; in the PCM/S, we fix d and vary Q_s to obtain different s . By (3.7) and (3.8) we only have $s = d(2Q_{cp} + 1)$ instead of $s = d^{2Q_{cp}}$ in the PCM/CP and dQ_s instead of $s = d^{3Q_s}$ in the PCM/S. However, we still plot the error versus $s = d^{2Q_{cp}}$ in the PCM/CP and versus $s = d^{3Q_s}$ in the PCM/S to investigate the PCM method in case

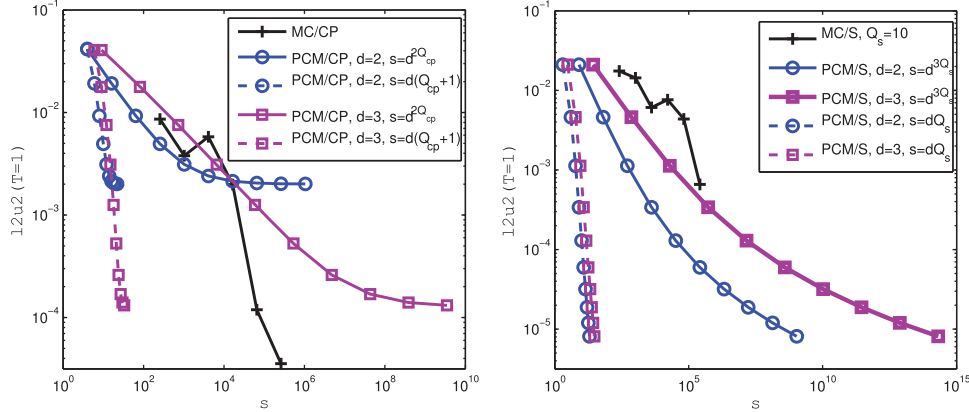


FIG. 4. PCM vs. MC: error $l2u2(T=1)$ of the solution for (1.1) versus the number of samples s obtained by MC/CP and PCM/CP with $\delta = 0.01$ (left) and MC/S with $Q_s = 10$ and PCM/S (right). $T = 1$, $c = 0.1$, $\alpha = 0.5$, $\lambda = 1$, $\epsilon = 0.1$, $\mu = 2$ (left and right). Spatial discretization: $N_x = 500$ Fourier collocation points on $[0, 2]$ (left and right); temporal discretization: first-order Euler scheme in (3.5) with time steps $\Delta t = 1 \times 10^{-5}$ (left and right). In both MC/CP and PCM/CP, $RelTol = 1 \times 10^{-8}$ for integration in $U(\delta)$.

the dimension of the random space cannot be reduced. With the dimension reduction, PCM/CP and PCM/S outperform the convergence of MC/CP and MC/S drastically; without the dimension reduction, the PCM/S seems to be still more accurate than the MC/S, however the slope of convergence of PCM/CP slows down for a larger $s = d^{2Q_{cp}}$. We also observe during the numerical experiment that the error is clearly decreased when we increase Q_s or Q_{cp} but it is not as clear when we increase d from 2 to 3.

4. Simulation of overdamped Langevin equations with TαS white noises.

In this section, we will present two methods for simulating the statistics for (1.2) by solving the corresponding generalized FP equation. In the first method, we solve for the density by approximating the TαS process L_t by a CP process, while in the second method, we solve a TFPDE. We will compare these two FP equation approaches with the previous MC and PCM methods via the empirical histograms and errors of moments.

4.1. Generalized FP equations for overdamped Langevin equations with TαS white noises. It is known that for any overdamped Langevin equation with a Lévy white noise η_t ,

$$(4.1) \quad dx(t) = f(x(t), t)dt + d\eta_t(\omega), \quad x(0) = x_0,$$

the PDF of the solution $P(x, t)$ satisfies the following generalized FP equation [12]

$$(4.2) \quad \frac{\partial}{\partial t}P(x, t) = -\frac{\partial}{\partial x} \left[f(x, t) P(x, t) \right] + \mathcal{F}^{-1} \left\{ P_k(t) \ln S_k \right\}.$$

S_k is the characteristic function (ch.f.) of the process η_t at time $t = 1$, as $S_k = \mathbf{E}[e^{-ik\eta_1}]$. We define the Fourier transformation for a function $v(x)$ as $\mathcal{F}\{v(x)\} = v_k = \int_{-\infty}^{+\infty} dx e^{-ikx} v(x)$. $P_k(t)$ is the ch.f. of $x(t)$, as $P_k(t) = \mathbf{E}[e^{-ikx(t)}]$. The inverse Fourier transformation is defined as $\mathcal{F}^{-1}\{v_k(x)\} = v = \frac{1}{2\pi} \int_{-\infty}^{+\infty} dx e^{ikx} v_k(x)$.

By the CP approximation with the jump truncation size δ of the T α S process L_t for (1.2), the density $P_{cp}(x, t)$ of the solution $x(t)$ satisfies [12]

$$(4.3) \quad \frac{\partial}{\partial t} P_{cp}(x, t) = \left[\sigma - 2U(\delta) \right] P_{cp}(x, t) + \sigma x \frac{\partial P_{cp}(x, t)}{\partial x} + \int_{-\infty}^{+\infty} dy P_{cp}(x-y, t) \frac{ce^{-\lambda|y|}}{|y|^{\alpha+1}}$$

with the initial condition $P_{cp}(x, 0) = \delta(x - x_0)$, where $U(\delta)$ is defined in (2.2).

We also obtain the generalized FP equations as TFPDE for the density $P_{ts}(x, t)$ directly from (4.2) without approximating L_t by a CP process for (1.2). Due to the fact that when $0 < \alpha < 1$ and $1 < \alpha < 2$, the ch.f.s for L_1, S_k , are in different forms, the density $P_{ts}(x, t)$ satisfies different equations for each case.

When $0 < \alpha < 1$, $S_k = \exp[-D\{(\lambda + ik)^\alpha - \lambda^\alpha\}]$ [11, 36], where $D = \frac{c}{\alpha}\Gamma(1 - \alpha)$, $\Gamma(t) = \int_0^{+\infty} x^{t-1} e^{-x} dx$, the density $P_{ts}(x, t)$ satisfies

$$(4.4) \quad \begin{aligned} \frac{\partial}{\partial t} P_{ts}(x, t) &= \frac{\partial}{\partial x} \left(\sigma x P_{ts}(x, t) \right) \\ &\quad - D(\alpha) \left(-_{\infty}D_x^{\alpha, \lambda} P_{ts}(x, t) + {}_x D_{+\infty}^{\alpha, \lambda} P_{ts}(x, t) \right), 0 < \alpha < 1, \end{aligned}$$

with the initial condition $P_{ts}(x, 0) = \delta(x - x_0)$. The left and right Riemann–Liouville tempered fractional derivatives are defined as [4, 36]:

$$(4.5) \quad -_{\infty}D_x^{\alpha, \lambda} f(x) = e^{-\lambda x} -_{\infty}D_x^\alpha [e^{\lambda x} f(x)] - \lambda^\alpha f(x), \quad 0 < \alpha < 1,$$

and

$$(4.6) \quad {}_x D_{+\infty}^{\alpha, \lambda} f(x) = e^{\lambda x} {}_x D_{+\infty}^\alpha [e^{-\lambda x} f(x)] - \lambda^\alpha f(x), \quad 0 < \alpha < 1.$$

In the above definitions, for $\alpha \in (n - 1, n)$ and $f(x)$ $(n - 1)$ -times continuously differentiable on $(-\infty, +\infty)$, $-_{\infty}D_x^\alpha$ and ${}_x D_{+\infty}^\alpha$ are left and right Riemann–Liouville fractional derivatives defined as [4]

$$(4.7) \quad -_{\infty}D_x^\alpha f(x) = \frac{1}{\Gamma(n - \alpha)} \frac{d^n}{dx^n} \int_{-\infty}^x \frac{f(\xi)}{(x - \xi)^{\alpha - n + 1}} d\xi,$$

$$(4.8) \quad {}_x D_{+\infty}^\alpha f(x) = \frac{(-1)^n}{\Gamma(n - \alpha)} \frac{d^n}{dx^n} \int_x^{+\infty} \frac{f(\xi)}{(\xi - x)^{\alpha - n + 1}} d\xi.$$

When $1 < \alpha < 2$, $S_k = \exp[D\{(\lambda + ik)^\alpha - \lambda^\alpha - ik\alpha\lambda^{\alpha-1}\}]$ [11, 36], where $D(\alpha) = \frac{c}{\alpha(\alpha-1)}\Gamma(2 - \alpha)$, the density $P_{ts}(x, t)$ satisfies

$$(4.9) \quad \begin{aligned} \frac{\partial}{\partial t} P_{ts}(x, t) &= \frac{\partial}{\partial x} \left(\sigma x P_{ts}(x, t) \right) \\ &\quad + D(\alpha) \left(-_{\infty}D_x^{\alpha, \lambda} P_{ts}(x, t) + {}_x D_{+\infty}^{\alpha, \lambda} P_{ts}(x, t) \right), 1 < \alpha < 2, \end{aligned}$$

with the initial condition $P_{ts}(x, 0) = \delta(x - x_0)$. The left and right Riemann–Liouville tempered fractional derivatives are defined as [4, 36]

$$(4.10) \quad -_{\infty}D_x^{\alpha, \lambda} f(x) = e^{-\lambda x} -_{\infty}D_x^\alpha [e^{\lambda x} f(x)] - \lambda^\alpha f(x) - \alpha\lambda^{\alpha-1} f'(x), \quad 1 < \alpha < 2,$$

and

$$(4.11) \quad {}_x D_{+\infty}^{\alpha, \lambda} f(x) = e^{\lambda x} {}_x D_{+\infty}^\alpha [e^{-\lambda x} f(x)] - \lambda^\alpha f(x) + \alpha\lambda^{\alpha-1} f'(x), \quad 1 < \alpha < 2.$$

The left and right Riemann–Liouville fractional derivatives ${}_{-\infty}D_x^\alpha$ and ${}_xD_{+\infty}^\alpha$ can be numerically implemented via the *Grünwald–Letnikov finite difference* form for $0 < \alpha < 1$ [35, 36, 44]:

$$(4.12) \quad \begin{cases} {}_{-\infty}D_x^\alpha f(x) = \lim_{h \rightarrow 0} \sum_{j=0}^{+\infty} \frac{1}{h^\alpha} W_j f(x - jh), & 0 < \alpha < 1, \\ {}_xD_{+\infty}^\alpha f(x) = \lim_{h \rightarrow 0} \sum_{j=0}^{+\infty} \frac{1}{h^\alpha} W_j f(x + jh), & 0 < \alpha < 1. \end{cases}$$

Here, ${}_{-\infty}D_x^\alpha$ and ${}_xD_{+\infty}^\alpha$ are implemented via the *shifted Grünwald–Letnikov finite difference* form for $1 < \alpha < 2$ [36, 44]:

$$(4.13) \quad \begin{cases} {}_{-\infty}D_x^\alpha f(x) = \lim_{h \rightarrow 0} \sum_{j=0}^{+\infty} \frac{1}{h^\alpha} W_j f(x - (j - 1)h), & 1 < \alpha < 2, \\ {}_xD_{+\infty}^\alpha f(x) = \lim_{h \rightarrow 0} \sum_{j=0}^{+\infty} \frac{1}{h^\alpha} W_j f(x + (j - 1)h), & 1 < \alpha < 2. \end{cases}$$

Note that $W_k = \binom{\alpha}{k} (-1)^k = \frac{\Gamma(k - \alpha)}{\Gamma(-\alpha)\Gamma(k + 1)}$ can be derived recursively via $W_0 = 1, W_1 = -\alpha, W_{k+1} = \frac{k - \alpha}{k + 1} W_k$. In the following numerical experiments, we will solve (4.4) and (4.9) by the aforementioned first-order numerical fractional finite difference scheme for spatial discretization on a sufficiently large domain $[-L, L]$ and fully implicit scheme for temporal discretization with time step Δt . Let us denote the approximated solution of $P_{ts}(x_i, t_n)$ as P_i^n . Let us denote $x_i = \frac{2L}{N_x} i - L = hi - L$, $i = 0, 1, \dots, N_x$, where h is the grid size. When $0 < \alpha < 1$, we use the following fully implicit discretization scheme for (4.4):

$$(4.14) \quad \frac{P_i^{n+1} - P_i^n}{\Delta t} = \left(\sigma + 2D(\alpha)\lambda^\alpha \right) P_i^{n+1} + \sigma x_i \frac{P_{i+1}^{n+1} - P_{i-1}^{n+1}}{2h} - \frac{D(\alpha)}{h^\alpha} e^{-\lambda x_i} \sum_{j=0}^i W_j e^{\lambda x_{i-j}} P_{i-j}^{n+1} - \frac{D(\alpha)}{h^\alpha} e^{\lambda x_i} \sum_{j=0}^{N_x-i} W_j e^{-\lambda x_{i+j} h} P_{i+j}^{n+1}.$$

When $1 < \alpha < 2$, we use the following fully implicit discretization scheme for (4.9):

$$(4.15) \quad \frac{P_i^{n+1} - P_i^n}{\Delta t} = \left(\sigma - 2D(\alpha)\lambda^\alpha \right) P_i^{n+1} + \sigma x_i \frac{P_{i+1}^{n+1} - P_{i-1}^{n+1}}{2h} + \frac{D(\alpha)}{h^\alpha} e^{-\lambda x_i} \sum_{j=0}^{i+1} W_j e^{\lambda x_{i-j+1}} P_{i-j+1}^{n+1} + \frac{D(\alpha)}{h^\alpha} e^{\lambda x_i} \sum_{j=0}^{N_x-i+1} W_j e^{-\lambda x_{i+j-1}} P_{i+j-1}^{n+1}.$$

In both the CP approximation and the series representation, we numerically approximate the initial condition by the delta sequences [1] either with *sinc* functions⁵

$$(4.16) \quad \delta_n^D = \frac{\sin(n\pi(x - x_0))}{\pi(x - x_0)}, \quad \lim_{n \rightarrow +\infty} \int_{-\infty}^{+\infty} \delta_n^D(x) f(x) dx = f(0),$$

or with Gaussian functions

$$(4.17) \quad \delta_n^G = \exp(-n(x - x_0)^2), \quad \lim_{n \rightarrow +\infty} \int_{-\infty}^{+\infty} \delta_n^G(x) f(x) dx = f(0).$$

⁵We approximate the initial condition by keeping the highest peak δ_n^D in the center and setting the value on the rest of the domain to be zeros. After that we normalize the area under the peak to be one.

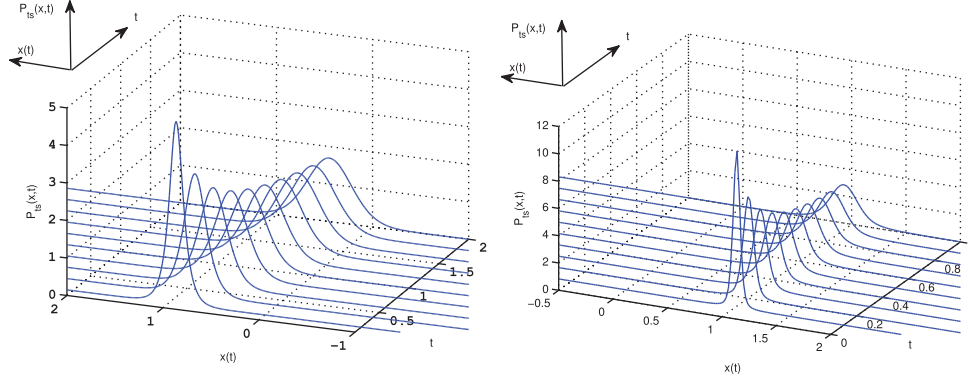


FIG. 5. Zoomed in density $P_{ts}(t, x)$ plots for the solution of (1.2) at different times obtained from solving (4.4) for $\alpha = 0.5$ (left) and (4.9) for $\alpha = 1.5$ (right): $\sigma = 0.4$, $x_0 = 1$, $c = 1$, $\lambda = 10$ (left); $\sigma = 0.1$, $x_0 = 1$, $c = 0.01$, $\lambda = 0.01$ (right). We have $N_x = 2000$ equidistant spatial points on $[-12, 12]$ (left); $N_x = 2000$ points on $[-20, 20]$ (right). Time step is $\Delta t = 1 \times 10^{-4}$ (left) and $\Delta t = 1 \times 10^{-5}$ (right). The initial conditions are approximated by δ_{20}^D (left and right).

In Figure 5 we simulate the density evolution for the solution of (1.2) obtained from the TFPDEs (4.4) and (4.9). The peak of the density moves towards smaller values of $x(t)$ due to the $-\sigma x(t; \omega) dt$ term. The noise $dL_t(\omega)$ changes the shape of the density.

The integral form of (1.2) is given by

$$(4.18) \quad x(t) = x_0 e^{-\sigma t} + e^{-\sigma t} \int_0^t e^{\sigma \tau} dL_\tau.$$

The mean and the second moment for the exact solution of (1.2) are

$$(4.19) \quad \mathbf{E}[x(t)] = x_0 e^{-\sigma t}$$

and

$$(4.20) \quad \mathbf{E}[x^2(t)] = x_0^2 e^{-2\sigma t} + \frac{c}{\sigma} (1 - e^{-2\sigma t}) \frac{\Gamma(2 - \alpha)}{\lambda^{2 - \alpha}}.$$

Let us define the errors of the first and the second moments to be

$$(4.21) \quad err_{1st}(t) = \frac{|\mathbf{E}[x_{num}(t)] - \mathbf{E}[x_{ex}(t)]|}{|\mathbf{E}[x_{ex}(t)]|}, \quad err_{2nd}(t) = \frac{|\mathbf{E}[x_{num}^2(t)] - \mathbf{E}[x_{ex}^2(t)]|}{|\mathbf{E}[x_{ex}^2(t)]|}.$$

4.2. Simulating density by CP approximation. Let us simulate the density of solution $x(t)$, $P_{cp}(x, t)$, in (1.2) by approximating the TaS process L_t by a CP process (density/CP) $\sum_{i=1}^{\infty} J_i^\delta \mathbf{1}_{t \leq T_i} + b^\delta t$ [11]. We solve (4.3) for $P_{cp}(x, t)$ via the second-order Runge-Kutta (RK2) for temporal discretization and via Fourier collocation on a sufficiently large domain $[-L, L]$ with N_x equidistant points $\{x_i = -L + \frac{2L}{N_x} i, i = 1, \dots, N_x\}$. For each x_i we simulate the integral in the last term $\int_{-\infty}^{+\infty} dy P_{cp}(x_i - y, t) \frac{c e^{-\lambda|y|}}{|y|^{\alpha+1}}$ via the trapezoid rule taking y to be all the other points on the grid other than x_i . We take $\delta = \frac{2L}{N_x}$ to include all the points on the Fourier collocation grid in this integration term.

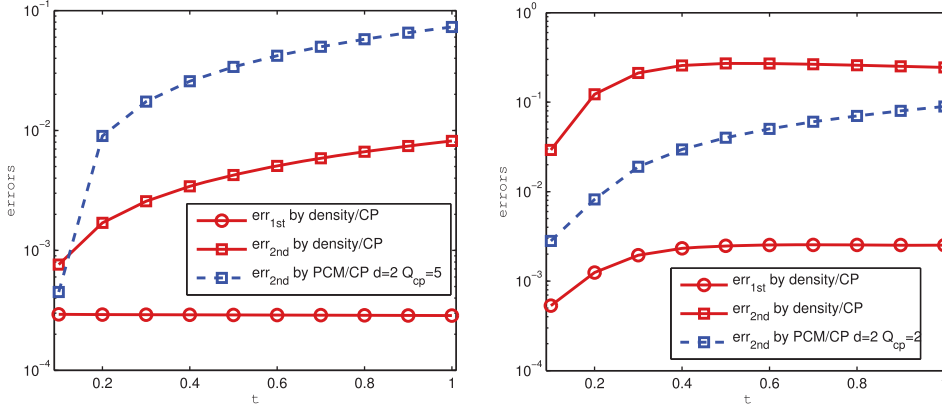


FIG. 6. Density/CP vs. PCM/CP with the same δ : errors err_{1st} and err_{2nd} of the solution for (1.2) versus time obtained by the density equation (4.3) with CP approximation and PCM/CP in (4.22). $c = 0.5$, $\alpha = 0.95$, $\lambda = 10$, $\sigma = 0.01$, $x_0 = 1$ (left); $c = 0.01$, $\alpha = 1.6$, $\lambda = 0.1$, $\sigma = 0.02$, $x_0 = 1$ (right). In the density/CP: RK2 with time steps $\Delta t = 2 \times 10^{-3}$, 1000 Fourier collocation points on $[-12, 12]$ in space, $\delta = 0.012$, $RelTol = 1 \times 10^{-8}$ for $U(\delta)$, and initial condition as δ_{20}^D (left and right). In the PCM/CP: the same $\delta = 0.012$ as in the density/CP.

We also simulate the moments for the solution of (1.2) by PCM/CP. Through the integral form (4.18) of the solution we directly sample the second moment of the solution by the following equation:

$$(4.22) \quad \mathbf{E}[x^2(t)] \approx x_0^2 e^{-2\sigma t} + e^{-2\sigma t} \mathbf{E}[(J_1^\delta)^2] \sum_{i=1}^{Q_{cp}} \mathbf{E}[e^{2\sigma T_i}].$$

We generate d collocation points for each of the RVs (J_1^δ and $\{T_i\}$) in (4.22) to obtain the moments.

In Figure 6, we plot the errors err_{1st} and err_{2nd} versus time for $0 < \alpha < 1$ and $1 < \alpha < 2$ of the density/CP and PCM/CP with the same jump truncation size δ . The error of the density/CP comes from (1) neglecting the jumps smaller than δ , (2) from evaluating $\int_{-\infty}^{+\infty} dy P_{cp}(x-y, t) \frac{ce^{-\lambda|y|}}{|y|^{\alpha+1}}$ by the trapezoid rule, (3) from numerical integration to calculate $U(\delta)$, and (4) from the delta sequence approximation of the initial condition. The error of the PCM/CP comes from (1) the jump truncation up to size δ , (2) the finite number Q_{cp} terms we consider in the CP approximation, (3) numerical integration for each $\mathbf{E}[(J_1^\delta)^2]$ and $\mathbf{E}[e^{2\sigma T_i}]$, and (4) the error from the long-term integration in the generalized polynomial chaos resulting from the fact that only a finite number of polynomial modes is considered and the error accumulates with respect to time (an error due to random frequencies) [53]. First, we observe that the error growth with time from the PCM/CP is faster than the density/CP for both plots in Figure 6. Then, we observe in Figure 6 that when L_t has more larger jumps ($\lambda = 0.1$, right), the PCM/CP with only $Q_{cp} = 2$ is more accurate than the density/CP with the same $\delta = 0.012$. (Larger values of Q_{cp} maintain the same level of accuracy with $Q_{cp} = 2$ or 5 here because the error is mainly determined by the choice of δ .)

4.3. Simulating density by TFPDEs. As an alternative method to simulate the density of the solution for (1.2), we will simulate the density $P_{ts}(x, t)$ by solving

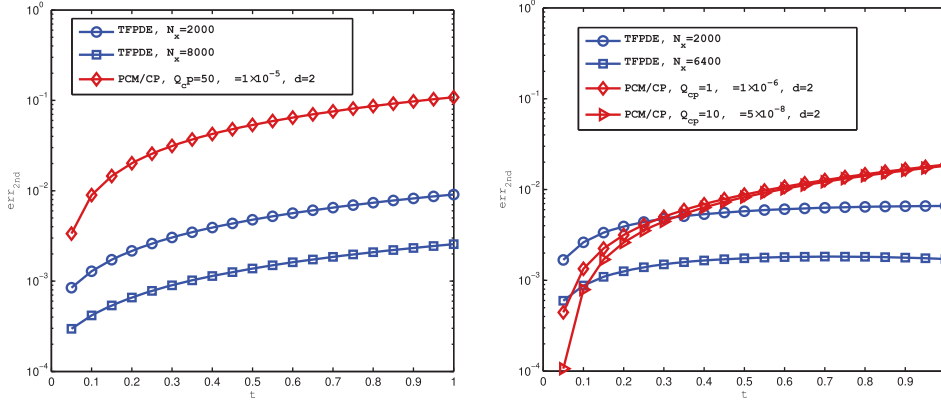


FIG. 7. TFPDE vs. PCM/CP: error err_{2nd} of the solution for (1.2) versus time with $\lambda = 10$ (left) and $\lambda = 1$ (right). Problems we are solving: $\alpha = 0.5$, $c = 2$, $\sigma = 0.1$, $x_0 = 1$ (left and right). For PCM/CP, $RelTol = 1 \times 10^{-8}$ for $U(\delta)$ (left and right). For the TFPDE, finite difference scheme in (4.14) with $\Delta t = 2.5 \times 10^{-5}$, N_x equidistant points on $[-12, 12]$, initial condition given by δ_{40}^D (left and right).

the TFPDEs (4.4) for $0 < \alpha < 1$ and (4.9) for $1 < \alpha < 2$. The corresponding finite difference schemes are given in (4.14) and (4.15).

In Figure 7, we plot the errors for the second moments versus time both by the PCM/CP and the TFPDEs. In the TFPDEs, we solve (4.4) and (4.9) by the finite difference schemes given in (4.14) and (4.15). The error of the TFPDEs mainly comes from (1) approximating the initial condition by delta sequences, and (2) temporal or spatial errors from solving (4.4) and (4.9).

In Figure 7 we experiment with $\lambda = 10$ (left, with fewer larger jumps) and with $\lambda = 1$ (right, with more larger jumps). First, we observe that with the same resolution for $x(t)$ ($N_x = 2000$ on $[-12, 12]$) and temporal resolution ($\Delta t = 2.5 \times 10^{-5}$), the err_{2nd} errors from the TFPDE method grow slower when $\lambda = 1$ than $\lambda = 10$, because a more refined grid is required to resolve the behavior of more smaller jumps (larger λ) between different values of $x(t)$. Second, we observe that the error from the PCM/CP grows slightly faster than the TFPDE method. In PCM/CP, the error from the long-term integration is inevitable with a fixed number of collocation points d . Third, without the dimension reduction in the PCM/CP (if we compute it on $d^{2Q_{cp}}$ points rather than $d(Q_{cp} + 1)$ points), the TFPDE consumes much less CPU time than the PCM/CP with a higher accuracy.

In Figure 8, we plot the density $P_{st}(x, t)$ obtained from the TFPDEs in (4.4) and (4.9) at two different final time values T and the empirical histograms obtained from the MC/CP with the first-order Euler scheme

$$(4.23) \quad x^{n+1} - x^n = -\sigma x^n \Delta t + (L_{t^{n+1}} - L_{t^n}).$$

Although we do not have the exact formula for the distribution of $x(t)$, we observe that the density from MC/CP matches the density from TFPDEs, indicated by the one-sample K-S test defined in (2.6).

5. Conclusions. In this paper we first compared the CP approximation and the series representation for a TaS by matching the empirical histogram of an IG subordinator with its known distribution. The one-sample K-S test values indicated

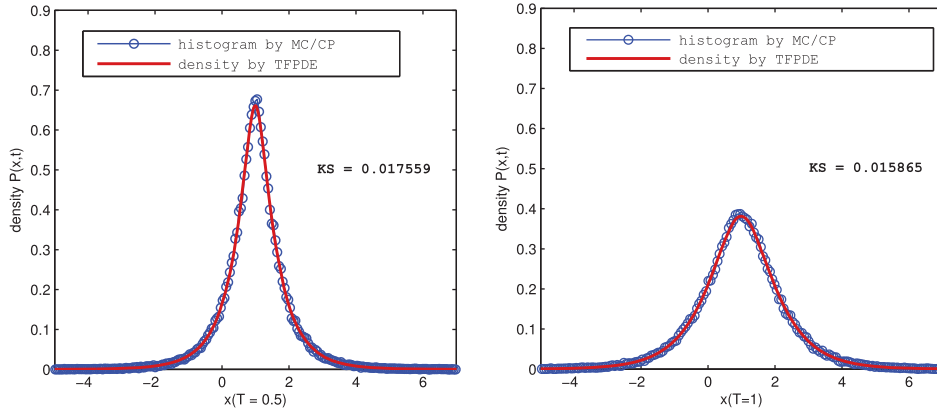


FIG. 8. Zoomed in plots for the density $P_{ts}(x, T)$ by solving the TFPDE (4.4) and the empirical histogram by MC/CP at $T = 0.5$ (left) and $T = 1$ (right): $\alpha = 0.5$, $c = 1$, $\lambda = 1$, $x_0 = 1$, and $\sigma = 0.01$ (left and right). In the MC/CP, sample size $s = 10^5$, 316 bins, $\delta = 0.01$, $RelTol = 1 \times 10^{-8}$ for $U(\delta)$, time step $\Delta t = 1 \times 10^{-3}$ (left and right). In the TFPDE, finite difference scheme given in (4.14) with $\Delta t = 1 \times 10^{-5}$ in time, $N_x = 2000$ equidistant points on $[-12, 12]$ in space, and the initial conditions are approximated by δ_{40}^D (left and right). We perform the one-sample K-S tests here to test how the two methods match.

a better fitting between the histogram and the distribution if we decreased the jump truncation size δ in the CP approximation and increased the number of terms Q_s in the series representation. When the cost is limited (large δ , small Q_s , the CP approximation), the large jumps are better approximated by the CP approximation.

Next we simulated the moment statistics for stochastic reaction-diffusion equations with additive $T\alpha S$ white noises, via four stochastic simulation methods: MC/CP, MC/S, PCM/CP, and PCM/S. First, in a comparison between the MC/CP and the MC/S, we observed that for almost the same accuracy, MC/CP costs less CPU time than the MC/S. We also observed that in the MC/CP, decreasing δ was more effective in reducing the error when the tail of the Lévy measure of the $T\alpha S$ process was more tempered. Second, in a comparison between the PCM/CP and the PCM/S, we observed that for a smaller sample size the PCM/CP converged faster because it captured the feature of larger jumps faster than the PCM/S, while for a larger sample size the PCM/S converged faster than the PCM/CP. However, the convergence of both PCM/CP and PCM/S slows down for higher accuracy due to the limitations discussed in section 3.2. We also introduced a dimension reduction in the PCM/CP and the PCM/S for this problem in Section 3.2. Third, we compared the efficiency between MC/CP and PCM/CP, and between MC/S and PCM/S. With the dimension reduction the PCM outperforms the efficiency of MC dramatically in evaluating the moment statistics. Without the dimension reduction, the PCM/S still outperforms the efficiency of MC/S for the same accuracy.

Subsequently, we simulated the stochastic overdamped Langevin equations with additive $T\alpha S$ white noises. We provided two different ways of simulating the generalized FP equations that describe the density of the solution: first we solved the generalized FP equation as an integral equation by approximating the $T\alpha S$ process as CP processes; then we solved the generalized FP equations as TFPDEs, in different forms for $0 < \alpha < 1$ and $1 < \alpha < 2$. The integral equations served as a good tool to predict the moment statistics in section 4.2. We observed that the TFPDEs provided more accurate moment statistics than the PCM/CP with much less compu-

tational cost without dimensional reduction in the PCM/CP. We also observed that the empirical histogram via MC/CP matches the PDF from the TFPDEs.

Finally, we want to point out that the four stochastic simulation methods (MC/CP, MC/S, PCM/CP, PCM/S) and the simulation of the generalized FP equations are not restricted to SPDEs with T α S processes, but they are applicable to SPDEs with any Lévy jump processes with known Lévy measures. In this paper we aim to develop new methods in relatively simple models with additive noise but in the future we will address nonlinear dynamics and multiplicative noise.

Appendix A. Algorithm to generate RVs with distribution $p^\delta(x) = \frac{1}{U(\delta)} \frac{ce^{\lambda x}}{x^{\alpha+1}} \mathbf{I}_{x \geq \delta}$ for CP approximation [13]. The distribution $p^\delta(x)$ can be bounded by

$$(A.1) \quad p^\delta(x) \leq \frac{\delta^{-\alpha} e^{-\lambda \delta}}{\alpha U(\delta)} f^\delta(x),$$

where $f^\delta(x) = \frac{\alpha \delta^{-\alpha}}{x^{\alpha+1}} \mathbf{I}_{x \geq \delta}$. The algorithm is [11, 13] the following.

ALGORITHM 1. GENERATE RVs WITH DISTRIBUTION $p^\delta(x) = \frac{1}{U(\delta)} \frac{ce^{\lambda x}}{x^{\alpha+1}} \mathbf{I}_{x \geq \delta}$.

REPEAT

Generate RVs W and V : independent and uniformly distributed on $[0, 1]$

Set $X = \delta W^{-1/\alpha}$

Set $T = \frac{f^\delta(X) \delta^{-\alpha} e^{-\lambda \delta}}{p^\delta(X) \alpha U(\delta)}$

UNTIL $VT \leq 1$

RETURN X .

Appendix B. Algorithm for CP processes [11]. Here we describe how to simulate the trajectories of a CP process with intensity $U(\delta)$ and jump size distribution $\frac{\nu^\delta(x)}{U(\delta)}$, on a simulation time domain $[0, T]$ at time t . The algorithm to generate sample paths for CP processes is given in Algorithm 2.

ALGORITHM 2. ALGORITHM FOR CP PROCESSES WITHOUT A DRIFT.

- Simulate an RV N from Poisson distribution with parameter $U(\delta)T$, as the total number of jumps on the interval $[0, T]$.
 - Simulate N independent RVs, T_i , uniformly distributed on the interval $[0, T]$, as jump times.
 - Simulate N jump sizes, Y_i with distribution $\frac{\nu^\delta(x)}{U(\delta)}$.
 - Then the trajectory at time t is given by $\sum_{i=1}^N \mathbf{I}_{T_i \leq t} Y_i$.
-

Appendix C. PDF of $[(\frac{\alpha \Gamma_j}{2cT})^{-1/\alpha} \wedge \eta_j \xi_j^{1/\alpha}]$ in series representation (2.3).

Let us denote $A_j = (\frac{\alpha \Gamma_j}{2cT})^{-1/\alpha}$ and $B_j = \eta_j \xi_j^{1/\alpha}$ for a fixed $j \in \{1, 2, 3, \dots\}$.

The distribution of A_j is calculated by the following:

$$(C.1) \quad F_{A_j}(A) = \mathbf{P} \left(\left(\frac{\alpha \Gamma_j}{2cT} \right)^{-1/\alpha} \leq A \right) = \mathbf{P} \left(\Gamma_j \geq \frac{2cT}{\alpha A^\alpha} \right) = \int_{\frac{2cT}{\alpha A^\alpha}}^{+\infty} \frac{e^{-x} x^{-1+j}}{\Gamma(j)} dx.$$

Therefore, the distribution of A is

$$(C.2) \quad f_{A_j}(A) = \frac{dF_A}{dA} = \frac{2cT}{\Gamma(j) A^{\alpha+1}} e^{-\frac{2cT}{\alpha A^\alpha}} \left(\frac{2cT}{\alpha A^\alpha} \right)^{-1+j}.$$

The distribution of B_j is derived by product distribution:

$$(C.3) \quad f_{B_j}(B) = \alpha\lambda \int_0^1 x^{\alpha-2} e^{-\lambda B/x} dx = (\alpha\lambda)(\lambda B)^{\alpha-1} \int_{\lambda B}^\infty t^{-\alpha} e^{-t} dt;$$

when $\alpha \neq 1$, it can be written as incomplete Gamma functions.

Therefore, the distribution of $[A_j \wedge B_j]$ is given by

$$(C.4) \quad f_{A_j \wedge B_j}(x) = f_{A_j}(x) \left(1 - F_{B_j}(x)\right) + f_{B_j}(x) \left(1 - F_{A_j}(x)\right).$$

When $0 < \alpha < 1$,

$$(C.5) \quad f_{A_j \wedge B_j}(x) = \left(\frac{\alpha}{x\Gamma(j)} e^{-t^j} \Big|_{t=\frac{2cT}{\alpha x^\alpha}}\right) \left[\alpha\Gamma(1-\alpha)\lambda^\alpha \int_x^{+\infty} (1 - \gamma_{inc}(\lambda z, 1-\alpha)) z^{\alpha-1} dz \right] + \left[\alpha\Gamma(1-\alpha)\lambda^\alpha (1 - \gamma_{inc}(\lambda x, 1-\alpha)x^{\alpha-1}) \right] \gamma_{inc}\left(\frac{2cT}{\alpha x^\alpha}, j\right).$$

When $1 < \alpha < 2$,

$$(C.6) \quad f_{A_j \wedge B_j}(x) = \left(\frac{\alpha}{x\Gamma(j)} e^{-t^j} \Big|_{t=\frac{2cT}{\alpha x^\alpha}}\right) \left[\int_x^{+\infty} f_{B_j}(z) dz \right] + f_{B_j}(x) \gamma_{inc}\left(\frac{2cT}{\alpha x^\alpha}, j\right).$$

Here the incomplete Gamma function $\gamma_{inc}(a, b)$ is defined as

$$(C.7) \quad \gamma_{inc}(a, b) = \frac{1}{\Gamma(a)} \int_0^b e^{-t} t^{a-1} dt.$$

Appendix D. Generation of orthogonal polynomials for arbitrary discrete measure with finite moments [42, 56]. Here we introduce how to generate orthogonal polynomials for a given measure out of its moments. Let ρ be a positive measure with infinite support $S(\rho) \subset \mathbb{R}$ and finite moments at all orders, i.e.,

$$(D.1) \quad m_n = \int_S \xi^n \rho(d\xi) < \infty \quad \forall n \in \mathbb{N}_0,$$

as the n th-order moment, where $\mathbb{N}_0 = \{0, 1, 2, \dots\}$, and it is defined as a Riemann–Stieltjes integral. There exists one unique set of orthogonal monic polynomials $\{P_i\}_{i=0}^\infty$ with respect to the measure ρ such that

$$(D.2) \quad \int_S P_i(\xi) P_j(\xi) \rho(d\xi) = \delta_{ij} \gamma_i^{-2}, \quad i = 0, 1, 2, \dots,$$

where $\gamma_i \neq 0$ are constants. The coefficients of the d th-order polynomial $P_d(\xi) = \sum_{i=0}^d a_i \xi^i$ are determined by the following linear system

$$(D.3) \quad \begin{pmatrix} m_0 & m_1 & \dots & m_d \\ m_1 & m_2 & \dots & m_{d+1} \\ \dots & \dots & \dots & \dots \\ m_{d-1} & m_d & \dots & m_{2d-1} \\ 0 & 0 & \dots & 1 \end{pmatrix} \begin{pmatrix} a_0 \\ a_1 \\ \dots \\ a_{d-1} \\ a_d \end{pmatrix} = \begin{pmatrix} 0 \\ 0 \\ \dots \\ 0 \\ 1 \end{pmatrix},$$

where the $(d + 1)$ by $(d + 1)$ Vandermonde matrix needs to be inverted.

REFERENCES

- [1] G. ARFKEN, *Mathematical Methods for Physicists*, 3rd ed., Academic Press, Orlando, FL, 1985.
- [2] S. ASMUSSEN AND J. ROSÍNSKI, *Approximations of small jumps of Lévy processes with a view towards simulation*, J. Appl. Probab., 38 (2001), pp. 482–493.
- [3] I. BABUŠKA, F. NOBILE, AND R. TEMPONE, *A stochastic collocation method for elliptic partial differential equations with random input data*, SIAM Rev., 52 (2010), pp. 317–355.
- [4] B. BAEUMER AND M. MEERSCHAERT, *Tempered stable Lévy motion and transient superdiffusion*, J. Comput. Appl. Math., 233 (2010), pp. 2438–2448.
- [5] F.E. BENTH AND A. LØKKA, *Anticipative calculus for Lévy processes and stochastic differential equations*, Stochastics Stochastics Rep., 76 (2004), pp. 191–211.
- [6] J. BERTOIN, *Lévy Processes*, Cambridge University Press, Cambridge, 1996.
- [7] M.L. BIANCHI, S.T. RACHEV, Y.S. KIM, AND F.J. FABOZZI, *Tempered stable distributions and processes in finance: Numerical analysis*, in Mathematical and Statistical Methods for Actuarial Sciences and Finance, Springer, Dordrecht, 2010, pp. 33–42.
- [8] L. BONDESSON, *On simulation from infinitely divisible distributions*, Adv. Appl. Probab., 14 (1982), pp. 855–869.
- [9] P. CARR, H. GEMAN, D.B. MADAN, AND M. YOR, *The fine structure of asset returns: An empirical investigation*, J. Bus., 75 (2002), pp. 303–325.
- [10] P. CARR, H. GEMAN, D.B. MADAN, AND M. YOR, *Stochastic volatility for Lévy processes*, Math. Finance, 13 (2003), pp. 345–382.
- [11] R. CONT, P. TANKOV, *Financial Modelling with Jump Processes*, Chapman & Hall/CRC Press, Boca Raton, FL, 2004.
- [12] S.I. DENISOV, W. HORSTHEMKE, AND P. HÄNGGI, *Generalized Fokker-Planck equation: Derivation and exact solutions*, Eur. Phys. J. B Condens. Matter Phys., 68 (2009), pp. 567–575.
- [13] L. DEVROYE, *Non-Uniform Random Variate Generation*, Springer, New York, 1986.
- [14] T.S. FERGUSON AND M.J. KLASS, *A representation of independent increment processes without Gaussian components*, Ann. Math. Statist., 43 (1972), pp. 1634–1643.
- [15] C.W. GARDINER, *Handbook of Stochastic Methods*, 2nd ed., Springer-Verlag, Berlin, 1990.
- [16] W. GAUTSCHI, *Construction of Gauss-Christoffel quadrature formulas*, Math. Comp., 22 (102) (1968), pp. 251–270.
- [17] W. GAUTSCHI, *On generating orthogonal polynomials*, SIAM J. Sci. Stat. Comp., 3 (1982), pp. 289–317.
- [18] H.U. GERBER AND S.W. ELIAS, *Option pricing by Esscher transforms*, Trans. Soc. Actuaries, 46 (1994), pp. 99–191.
- [19] G. H. GOLUB AND J. H. WELSCH, *Calculation of Gauss quadrature rules*, Math. Comp., 23 (1969), pp. 221–230.
- [20] H. GRABERT, *Projection Operator Techniques in Nonequilibrium Statistical Mechanics*, Springer Tracts Modern Phys. 95, Springer-Verlag, Berlin, 1982.
- [21] J.S. HESTHAVEN, S. GOTTLIEB, AND D. GOTTLIEB, *Spectral Methods for Time-Dependent Problems*, Cambridge University Press, New York, 2007.
- [22] W. HORSTHEMKE AND R. LEFEVER, *Noise-Induced Transitions: Theory and Applications in Physics, Chemistry, and Biology*, 2nd ed., Springer Ser. Synergetics, Springer, Berlin, 2006.
- [23] N. IKEDA AND S. WATANABE, *Stochastic Differential Equations and Diffusion Processes*, North Holland, Amsterdam, 1981.
- [24] K. ITÔ, *Stochastic differential equations in a differentiable manifold*, Nagoya Math. J., 1 (1950), pp. 35–47.
- [25] K. ITÔ, *Spectral type of the shift transformation of differential processes and stationary increments*, Trans. Amer. Math. Soc., 81 (1956), pp. 253–263.
- [26] A.Y. KHINTCHINE, *Zur Theorie der unbeschränkt teilbaren Verteilungsgesetze*, Mat. Sb., 2 (1937), pp. 79–119.
- [27] I. KOPONEN, *Analytic approach to the problem of convergence of truncated Lévy flights towards the Gaussian stochastic process*, Phys. Rev. E (3), 52 (1995), pp. 1197–1199.
- [28] P. LANGEVIN, *Sur la théorie de mouvement Brownien*, C.R. Acad. Sci. Paris, 146 (1908), pp. 530–533.
- [29] R. LEPAGE, *Multidimensional infinitely divisible variables and processes Part II*, in Probability in Banach Spaces III, Lecture Notes Math. 860, Springer-Verlag, Berlin, 1980, pp. 279–284.
- [30] A. LØKKA, B. ØKSENDAL, AND F. PROSKE, *Stochastic partial differential equations driven by Lévy space-time white noise*, Ann. Appl. Probab., 14 (2004), pp. 1506–1528.
- [31] A. LØKKA AND F. PROSKE, *Infinite dimensional analysis of pure jump Lévy processes on the Poisson space*, Math. Scand., 98 (2006), pp. 237–261.
- [32] B. MANDELBROT, *The variation of certain speculative prices*, J. Bus., 36 (1963), pp. 394–419.

- [33] R.N. MANTEGNA AND H.E. STANLEY, *Stochastic process with ultraslow convergence to a Gaussian: The truncated Lévy flight*, Phys. Rev. Lett., 73 (1994), pp. 2946–2949.
- [34] F.J. MASSEY, *The Kolmogorov-Smirnov test for goodness of fit*, J. Amer. Statist. Assoc., 46 (1951), pp. 68–78.
- [35] M.M. MEERSCHAERT AND C. TADJERAN, *Finite difference approximations for fractional advection-dispersion flow equations*, J. Comput. Appl. Math., 172 (2004), pp. 65–77.
- [36] M.M. MEERSCHAERT AND A. SIKORSKII, *Stochastic Models for Fractional Calculus*, De Gruyter Stud. Math., 43, De Gruyter, Berlin, 2012.
- [37] G.D. NUNNO, B. ØKSENDAL, AND F. PROSKE, *Malliavin Calculus for Lévy Processes with Applications to Finance*, Springer, Berlin, 2009.
- [38] G.D. NUNNO, B. ØKSENDAL, AND F. PROSKE, *White noise analysis for Lévy processes*, J. Funct. Anal., 206 (2004), pp. 109–148.
- [39] E.A. NOVIKOV, *Infinitely divisible distributions in turbulence*, Phys. Rev. E (3), 50 (1994), pp. R3303–R3305.
- [40] B. ØKSENDAL, *Stochastic partial differential equations driven by multi-parameter white noise of Lévy processes*, Quart. Appl. Math., 66 (2008), pp. 521–537.
- [41] B. ØKSENDAL AND F. PROSKE, *White noise of Poisson random measure*, Potential Anal., 21 (2004), pp. 375–403.
- [42] S. OLADYSHKIN AND W. NOWAK, *Data-driven uncertainty quantification using the arbitrary polynomial chaos expansion*, Reliability Eng. System Safety, 106 (2012), pp. 179–190.
- [43] E. PLATEN AND N. BRUTI-LIBERATI, *Numerical Solution of Stochastic Differential Equations with Jumps in Finance*, Springer, Berlin, 2010.
- [44] I. PODLUBNY, *Fractional Differential Equations*, Academic Press, New York, 1999.
- [45] J. POIROT AND P. TANKOV, *Monte Carlo option pricing for tempered stable (CGMY) processes*, Asia-Pacific Financial Markets, 13 (2006), pp. 327–344.
- [46] P.E. PROTTER, *Stochastic Integration and Differential Equations*, 2nd ed., Springer, New York, 2005.
- [47] H. RISKEN, *The Fokker-Planck Equation*, 2nd ed., Springer-Verlag, Berlin, 1989.
- [48] J. ROSÍNSKI, *Series representations of Lévy processes from the perspective of point processes*, in Lévy Processes - Theory and Applications, O.E. Barndorff-Nielsen, T. Mikosch, and S.I. Resnick, eds., Birkhäuser, Boston, 2001, pp. 401–415.
- [49] J. ROSÍNSKI, *On series representations of infinitely divisible random vectors*, Ann. Probab., 18 (1990), pp. 405–430.
- [50] J. ROSÍNSKI, *Series Representations of Infinitely Divisible Random Vectors and a Generalized Shot Noise in Banach Spaces*, Center for Stochastic Processes, Technical report 195, University of North Carolina at Chapel Hill, Chapel Hill, NC, 1987.
- [51] J. ROSÍNSKI, *Tempering stable processes*, Stochastic Process Appl., 117 (2007), pp. 677–707.
- [52] S. KEN-ITI, *Lévy Processes and Infinitely Divisible Distributions*, Cambridge University Press, Cambridge, 1999.
- [53] X. WAN AND G.E. KARNIADAKIS, *Long-term behavior of polynomial chaos in stochastic flow simulations*, Comput. Methods Appl. Mech. Engrg., 195 (2006), pp. 5582–5596.
- [54] W.N. VENABLES AND B.D. RIPLEY, *Modern Applied Statistics with S*, 4th ed., Springer, New York, 2002.
- [55] D. XIU AND J.S. HESTHAVEN, *High order collocation methods for differential equations with random inputs*, SIAM J. Sci. Comput., 27 (2005), pp. 1118–1139.
- [56] M. ZHENG, X. WAN, AND G.E. KARNIADAKIS, *Adaptive multi-element polynomial chaos with discrete measure: Algorithms and application to SPDEs*, Appl. Numer. Math., 90 (2015), pp. 91–110.